

# Comparing Controllers for Dynamic Positioning of Ships in Extreme Seas

Ole M. R. Rabanal\* Astrid H. Brodtkorb\*\* Morten Breivik\*

\* *Department of Engineering Cybernetics (e-mail: ole.roeste@gmail.com, morten.breivik@ieee.org).*

\*\* *Centre for Autonomous Marine Operations and Systems, Department of Marine Technology (e-mail: astrid.h.brodtkorb@ntnu.no).*

*Norwegian University of Science and Technology (NTNU), NO-7491, Trondheim, Norway*

---

**Abstract:** This paper considers the design, implementation and experimental verification of two controllers for ship station keeping in extreme seas. In particular, the performance of two dynamic positioning controllers are compared, namely a sliding mode controller and a PID controller with acceleration feedback. The former has been tested in extreme seas before because the acceleration feedback term virtually increases the inertia of the ship, making it less sensitive to large wave loads. Sliding mode control is chosen because of its robustness to parameter uncertainties such as frequency dependency of added mass and damping. Model-scale experiments are performed in the Marine Cybernetics Laboratory at the Norwegian University of Science and Technology. The performance is measured by new performance metrics combining the energy consumption from thrusters onboard the ship with position and heading precision.

*Keywords:* Dynamic positioning, station keeping, extreme seas, PID, acceleration feedback, sliding mode control, performance metrics, model-scale experiments, energy efficiency

---

## 1. INTRODUCTION

Marine operations are becoming more challenging due to operations in deeper waters, further from shore, where the sea state often can be characterized as extreme, with large waves and wind gusts. With such environmental effects, the need for dynamic positioning (DP) vessels with enhanced positioning capabilities increases. The authors are therefore motivated to find a safer, smarter and greener DP algorithm for maintaining safety of personnel and cargo while at the same time ensuring an energy efficient operation. In extreme seas, large motion couplings in six degrees of freedom (DOF) occur and it is therefore important to have a robust controller.

Sea states with significant wave height  $H_s \geq 3.5$  m and peak period of waves  $T_p \geq 10$  s are here referred to as extreme seas. Such sea states, or higher, occur roughly 30% of the time in the Northern North Atlantic. When extreme seas occur, waves are higher and have longer periods so that the wave-frequency (WF) motions are found in the same frequency regime as the low-frequency (LF) motions of the vessel. This will cause a challenge for an estimator separating the LF from the WF motions using a wave filter, because the wave filter removes important LF vessel motions that the controller should compensate for. To solve this problem, Sørensen et al. (2002) proposed to neglect the wave filter for extreme seas in order to maintain performance and stability. This has been tested by Nguyen et al. (2007) and Brodtkorb et al. (2014) with the use of hybrid controllers in simulations and experiments with a model-scale ship. The hybrid controller

implemented in both works include proportional-integral-derivative control with acceleration feedback (PID-AFB) and a nonlinear passive observer (NPO) without wave filtering. By comparing simulations of the hybrid controller with a single PID controller with wave filtering, in a sea state varying from calm to extreme seas, the hybrid controller provided best performance. A PID-AFB controller was first proposed by Lindegaard (2003), where a virtual inertia is added to the physical inertia and increased by using feedback of the measured acceleration of the system.

Sliding mode control (SMC) is recognized as an efficient tool for designing robust controllers for complex high-order nonlinear dynamic plants operating under uncertain conditions. SMC has been adapted and used for multiple-input, multiple-output (MIMO) nonlinear systems by Slotine and Li (1991) and extended by Fossen and Foss (1991), with the idea of designing a robust controller in the case of unmodeled dynamics and modeling inaccuracies of parameters such as inertia, external loads and actuators. The robustness of the SMC algorithm is here achieved by introducing uncertainties to the parameters added mass and damping.

The main contributions of this paper include the implementation and experimental testing of two DP control algorithms on a model-scale ship and evaluating performance by applying new performance metrics. The performance metrics include the pose (position and heading) accuracy and energy consumption by the thrusters. Experiments with the ship model in different sea states were conducted in the Marine Cybernetics Laboratory

(MCLab) comparing the performance of PID-AFB and SMC in DP when exposed to extreme seas. More details from the experiments can be found in (Rabanal, 2015).

The paper is organized as follows: Section 2 presents the mathematical modeling of the ship and a model-based observer; Section 3 describes the design of the PID-AFB and SMC controllers; Section 4 describes the lab setup, test cases, parameter tuning and performance metrics; Section 5 presents the results and discussion, Section 6 concludes the paper and the acknowledgments are found in Section 7.

## 2. MATHEMATICAL MODELING

This section considers mathematical modeling of marine vessels and a model-based observer for extreme seas.

### 2.1 Control Plant Model (CPM)

A control plant model (CPM) is a mathematical model describing only the most important physical properties of a dynamical process and is used for model-based observer and controller design Sørensen (2013).

In sea states with peak wave periods from 5-9 seconds, corresponding to sea state codes calm-rough (Price and Bishop, 1974), a DP control system counteracts low-frequency (LF) wave motions caused by wind, current and slowly-varying wave loads. It is common to filter out the wave-frequency (WF) vessel motions from the measurements caused by first-order wave loads in order to avoid wear and tear of the propulsion system.

When the vessel experiences extreme seas, such an observer wave filter will remove important LF vessel motions, leading to poor estimates of the pose. Maintaining pose when the vessel is experiencing motions due to large waves then becomes a challenge. Such waves have long periods and are most likely generated by wind (Fossen, 2011). Sørensen et al. (2002) proposes to solve this problem by reformulating the CPM by neglecting the WF model. When disabling the wave filter, the controller has to compensate for both LF and WF motions, which will cause more sudden movements and increased thrust in the corresponding directions.

A CPM for DP in extreme seas (Sørensen et al., 2002) is:

$$\dot{\boldsymbol{\eta}} = \mathbf{R}(\psi)\boldsymbol{\nu} \quad (1a)$$

$$\mathbf{M}\dot{\boldsymbol{\nu}} = -\mathbf{D}\boldsymbol{\nu} + \mathbf{R}^\top(\psi)\mathbf{b} + \boldsymbol{\tau} \quad (1b)$$

$$\dot{\mathbf{b}} = -\mathbf{T}_b^{-1}\mathbf{b} + \mathbf{E}_b\mathbf{w}_b \quad (1c)$$

$$\mathbf{y} = \boldsymbol{\eta} + \mathbf{v}, \quad (1d)$$

where  $\boldsymbol{\eta} \in \mathbb{R}^3$  is the position and heading (pose) vector and the velocity vector is written as  $\boldsymbol{\nu} \in \mathbb{R}^3$ . The rotation matrix  $\mathbf{R}(\psi) \in \mathbb{R}^{3 \times 3}$  transforms the velocity from the body-fixed to the north-east-down (NED) reference frame. A bias model with state  $\mathbf{b} \in \mathbb{R}^3$  represents slowly-varying environmental forces and is driven by the zero-mean Gaussian white noise vector  $\mathbf{w}_b \in \mathbb{R}^3$  with the disturbance scaling matrix  $\mathbf{E}_b \in \mathbb{R}^{3 \times 3}$ . In addition,  $\mathbf{T}_b \in \mathbb{R}^{3 \times 3}$  is a user-specified diagonal matrix of positive bias time constants. The matrix  $\mathbf{M} \in \mathbb{R}^{3 \times 3}$  is the inertia matrix consisting of the rigid-body and added-mass terms, while

linear damping is represented by the matrix  $\mathbf{D} \in \mathbb{R}^{3 \times 3}$ . The commanded forces and moment vector  $\boldsymbol{\tau} \in \mathbb{R}^3$  is generated by the controller, and the measurement from sensor output is written as  $\mathbf{y} \in \mathbb{R}^3$ . The measurement noise vector is  $\mathbf{v} \in \mathbb{R}^3$ .

### 2.2 Nonlinear Passive Observer (NPO)

The observer is an important part of a DP system because of its capabilities of state estimation and filtering. If sensors become faulty or too expensive, the observer can perform state estimation of non-measured states. If the vessel experiences signal losses because of sensor failure, one can use dead reckoning and trust the prediction model in the observer.

The following observer without wave filtering is proposed by Sørensen et al. (2002) for extreme seas:

$$\dot{\hat{\boldsymbol{\eta}}} = \mathbf{R}(\mathbf{y})\hat{\boldsymbol{\nu}} + \mathbf{K}_1\tilde{\mathbf{y}} \quad (2a)$$

$$\dot{\hat{\mathbf{b}}} = -\mathbf{T}_b^{-1}\hat{\mathbf{b}} + \mathbf{K}_2\tilde{\mathbf{y}} \quad (2b)$$

$$\mathbf{M}\dot{\hat{\boldsymbol{\nu}}} = -\mathbf{D}\hat{\boldsymbol{\nu}} + \mathbf{R}^\top(\mathbf{y})\hat{\mathbf{b}} + \boldsymbol{\tau} + \mathbf{R}^\top(\mathbf{y})\mathbf{K}_3\tilde{\mathbf{y}} \quad (2c)$$

$$\hat{\mathbf{y}} = \hat{\boldsymbol{\eta}}, \quad (2d)$$

where  $\hat{\boldsymbol{\eta}}$  and  $\hat{\boldsymbol{\nu}}$  are the estimated pose and velocity vectors,  $\hat{\mathbf{b}}$  is the estimated bias state,  $\hat{\mathbf{y}}$  is the estimated output, while matrices such as  $\mathbf{M}$  and  $\mathbf{D}$  are given above. The rotation matrix is written as  $\mathbf{R}(\mathbf{y}) = \mathbf{R}(\psi)$  and  $\mathbf{K}_1 \in \mathbb{R}^{3 \times 3}$ ,  $\mathbf{K}_2 \in \mathbb{R}^{3 \times 3}$  and  $\mathbf{K}_3 \in \mathbb{R}^{3 \times 3}$  are positive definite observer gain matrices.

## 3. CONTROLLER DESIGN

This section presents the control design of PID with acceleration feedback (PID-AFB) and sliding mode control (SMC) algorithms for generating the control input  $\boldsymbol{\tau}$ .

### 3.1 PID with Acceleration Feedback (PID-AFB)

This subsection is inspired by Fossen et al. (2002) and Lindgaard (2003). The PID-AFB controller is different from the conventional PID controller due to an extra inertia term  $\mathbf{K}_m$  that is fed back with measured acceleration and added to the system inertia matrix  $\mathbf{M}$ . This makes the system less sensitive to external disturbances and hence more robust. The control input  $\boldsymbol{\tau}$  from (1b) is generated by the following control law:

$$\boldsymbol{\tau} = \boldsymbol{\tau}_{PID-AFB} = \mathbf{R}^\top(\psi)\boldsymbol{\tau}_{PID} - \mathbf{K}_m\dot{\boldsymbol{\nu}}, \quad (3)$$

with

$$\boldsymbol{\tau}_{PID} = -\mathbf{K}_p\tilde{\boldsymbol{\eta}} - \mathbf{R}(\psi)\mathbf{K}_d\boldsymbol{\nu} - \mathbf{K}_i \int_0^t \tilde{\boldsymbol{\eta}}(\tau) d\tau. \quad (4)$$

The control objective is to force  $\tilde{\boldsymbol{\eta}} \rightarrow \mathbf{0}$  when  $t \rightarrow \infty$ , where  $\tilde{\boldsymbol{\eta}} = \boldsymbol{\eta} - \boldsymbol{\eta}_d$  is the error between the actual and desired pose. As the aim is station keeping, the desired pose is constant and  $\dot{\boldsymbol{\eta}}_d \approx \mathbf{0}$ . The positive definite gain matrices  $\mathbf{K}_p \in \mathbb{R}^{3 \times 3}$ ,  $\mathbf{K}_d \in \mathbb{R}^{3 \times 3}$  and  $\mathbf{K}_i \in \mathbb{R}^{3 \times 3}$  belong to the PID-part of the controller.

The AFB gain matrix  $\mathbf{K}_m \in \mathbb{R}^{3 \times 3}$  is chosen as proposed by Fossen et al. (2002) with  $\mathbf{K}_m = \mathbf{M}^* + \Delta\mathbf{K}$ , where  $\mathbf{M}^*$

is a modified inertia matrix  $\mathbf{M}^* = \begin{bmatrix} X_{\dot{u}} & 0 & 0 \\ 0 & Y_{\dot{v}} & 0 \\ 0 & N_{\dot{v}} - Y_{\dot{r}} & 0 \end{bmatrix}$  and

$\Delta \mathbf{K} = \Delta \mathbf{K}^\top$ . The AFB gain matrix is written as:

$$\mathbf{K}_m = \begin{bmatrix} K_{11} & K_{12} & 0 \\ K_{21} & K_{22} & 0 \\ K_{31} & K_{32} & 0 \end{bmatrix} = \begin{bmatrix} X_{\dot{u}} + \Delta K_{11} & 0 & 0 \\ 0 & Y_{\dot{v}} + \Delta K_{22} & 0 \\ 0 & N_{\dot{v}} - Y_{\dot{r}} & 0 \end{bmatrix} \quad (5)$$

where  $X_{\dot{u}}$ ,  $Y_{\dot{v}}$ ,  $N_{\dot{v}}$ ,  $Y_{\dot{r}}$  are hydrodynamic added-mass terms. For tuning advantages with DP, Fossen et al. (2002) proposes to choose  $\Delta K_{11} = \Delta K_{22} = \Delta K \geq 0$  which provides equal mass in the x- and y-directions such that the PID controller is independent of the heading angle. Consequently, a new virtual inertia  $\mathbf{H}$  is made:

$$\mathbf{H} = \mathbf{M} + \mathbf{K}_m = \mathbf{H}^\top > 0, \quad (6)$$

with

$$\mathbf{M} = \begin{bmatrix} m - X_{\dot{u}} & 0 & 0 \\ 0 & m - Y_{\dot{v}} & mx_g - Y_{\dot{r}} \\ 0 & mx_g - N_{\dot{v}} & I_z - N_{\dot{r}} \end{bmatrix} \quad (7)$$

and

$$\mathbf{H} = \begin{bmatrix} m + \Delta K & 0 & 0 \\ 0 & m + \Delta K & mx_g - Y_{\dot{r}} \\ 0 & mx_g - Y_{\dot{r}} & I_z - N_{\dot{r}} \end{bmatrix}. \quad (8)$$

The AFB gain matrix parameter  $\Delta K$  is measured in [kg] and  $K_{11}$ ,  $K_{12}$ ,  $K_{21}$ ,  $K_{22}$ ,  $K_{31}$  and  $K_{32}$  are chosen as shown in (5) such that  $\mathbf{H} = \mathbf{H}^\top > 0$ .

By inserting (3) into (1b), the resulting closed loop system becomes:

$$\mathbf{H}\dot{\boldsymbol{\nu}} + (\mathbf{D} + \mathbf{K}_d^*)\boldsymbol{\nu} + \mathbf{R}^\top(\psi)(\mathbf{K}_p\tilde{\boldsymbol{\eta}} + \mathbf{K}_i \int_0^t \tilde{\boldsymbol{\eta}}(\tau) d\tau) = \mathbf{R}^\top(\psi)\mathbf{b}, \quad (9)$$

where  $\mathbf{K}_d^* = \mathbf{R}^\top(\psi)\mathbf{K}_d\mathbf{R}(\psi)$ . For the following analysis, the integral action is assumed to cancel out the bias exactly. When integral action and bias are included, local asymptotic stability can be proven as described in Arimoto and Miyazaki (1984). The proposed Lyapunov function candidate is:

$$V = \frac{1}{2}\tilde{\boldsymbol{\eta}}^\top \mathbf{K}_p\tilde{\boldsymbol{\eta}} + \frac{1}{2}\boldsymbol{\nu}^\top \mathbf{H}\boldsymbol{\nu}. \quad (10)$$

Differentiating with respect to time and inserting (8) gives:

$$\dot{V} = \boldsymbol{\nu}^\top \mathbf{H}\dot{\boldsymbol{\nu}} + \tilde{\boldsymbol{\eta}}^\top \mathbf{K}_p\dot{\tilde{\boldsymbol{\eta}}} \quad (11)$$

$$= \boldsymbol{\nu}^\top (\mathbf{H}\dot{\boldsymbol{\nu}} + \mathbf{R}^\top(\psi)\mathbf{K}_p\tilde{\boldsymbol{\eta}}), \quad (12)$$

yielding  $\dot{V}$  negative semi-definite:

$$\dot{V} = -\boldsymbol{\nu}^\top [\mathbf{D} + \mathbf{K}_d^*]\boldsymbol{\nu} \leq 0, \quad \forall \boldsymbol{\nu} \neq \mathbf{0}. \quad (13)$$

Global asymptotically stability of the equilibrium point  $(\tilde{\boldsymbol{\eta}}, \boldsymbol{\nu}) = (\mathbf{0}, \mathbf{0})$  can be proven with Krasovskii-LaSalle's Theorem for PD control as shown in (Fossen, 2011).

### 3.2 Sliding Mode Control (SMC)

This section is inspired by Slotine and Li (1991), Fossen and Foss (1991), Fossen (2011) and Khalil (2002). The aim of the SMC algorithm is to account for parameter uncertainties in mass and damping, unmodeled dynamics, neglected time-delays, etc. (Slotine and Li, 1991).

First, a measure of tracking is defined:

$$\mathbf{s} := \dot{\tilde{\boldsymbol{\eta}}} + 2\Lambda\tilde{\boldsymbol{\eta}} + \Lambda^\top \Lambda \int_0^t \tilde{\boldsymbol{\eta}}(\tau) d\tau, \quad (14)$$

where  $\mathbf{s}$  is the sliding surface dependent on the pose error  $\tilde{\boldsymbol{\eta}}$  and the NED velocity error  $\dot{\tilde{\boldsymbol{\eta}}} = \dot{\boldsymbol{\eta}}$ . The tuning parameter  $\Lambda \in \mathbb{R}^{3 \times 3}$  with  $\Lambda > 0$  represents the bandwidth of the controller. Defining a virtual reference vector  $\boldsymbol{\eta}_r$  and rewriting (14):

$$\mathbf{s} = \dot{\boldsymbol{\eta}} - \dot{\boldsymbol{\eta}}_r, \quad (15)$$

$$\dot{\boldsymbol{\eta}}_r = \dot{\boldsymbol{\eta}}_d - 2\Lambda\tilde{\boldsymbol{\eta}} - \Lambda^\top \Lambda \int_0^t \tilde{\boldsymbol{\eta}}(\tau) d\tau, \quad (16)$$

so that

$$\dot{\mathbf{s}} = \ddot{\boldsymbol{\eta}} - \ddot{\boldsymbol{\eta}}_r. \quad (17)$$

When  $\mathbf{s} = \mathbf{0}$ , we have that (14) describes a sliding surface where  $\tilde{\boldsymbol{\eta}}$  converges exponentially to zero.

The equations of motion will now be described in the NED frame, as it is control of the pose that is of interest. The integral part in (14) is added separately to the control input in the implementation. The equations of motion are according to Fossen (2011, Chapter 7):

$$\mathbf{M}^*(\boldsymbol{\eta})\ddot{\boldsymbol{\eta}} + \mathbf{D}^*(\boldsymbol{\eta})\dot{\boldsymbol{\eta}} = \mathbf{b} + \boldsymbol{\tau}^*, \quad (18)$$

with  $\mathbf{M}^*(\boldsymbol{\eta}) = \mathbf{R}(\psi)\mathbf{M}\mathbf{R}^\top(\psi)$ ,  $\mathbf{D}^*(\boldsymbol{\eta}) = \mathbf{R}(\psi)\mathbf{D}\mathbf{R}^\top(\psi)$ ,  $\boldsymbol{\tau}^* = \mathbf{R}(\psi)\boldsymbol{\tau}_{SMC}$ , where  $\boldsymbol{\tau}_{SMC}$  is shown in (28).

Fossen and Foss (1991) derived a control law for MIMO SMC of underwater vehicles and the following is based on this work. The Lyapunov function candidate is chosen to be:

$$V = \frac{1}{2}\mathbf{s}^\top \mathbf{M}^* \mathbf{s}, \quad \mathbf{M}^* = (\mathbf{M}^*)^\top > 0, \quad (19)$$

where  $\mathbf{s}$  is the sliding surface in (14)-(16). By adding and subtracting  $\mathbf{s}^\top \mathbf{C}^* \mathbf{s}$ , the time derivative of (19) becomes:

$$\dot{V} = \mathbf{s}^\top \mathbf{M}^* \dot{\mathbf{s}} + \frac{1}{2}\mathbf{s}^\top \dot{\mathbf{M}}^* \mathbf{s} + \mathbf{s}^\top \mathbf{C}^* \mathbf{s} - \mathbf{s}^\top \mathbf{C}^* \mathbf{s} \quad (20)$$

Using the skew-symmetry property  $\mathbf{s}^\top (\dot{\mathbf{M}}^* - \mathbf{C}^*)\mathbf{s} = 0$ , we get the following for low velocities in station keeping:

$$\dot{V} = \mathbf{s}^\top \mathbf{M}^* \dot{\mathbf{s}}. \quad (21)$$

Inserting (17) into (21) yields:

$$\dot{V} = \mathbf{s}^\top \mathbf{M}^* (\ddot{\boldsymbol{\eta}} - \ddot{\boldsymbol{\eta}}_r) \quad (22)$$

$$= \mathbf{s}^\top (-\mathbf{M}^* \ddot{\boldsymbol{\eta}}_r - \mathbf{D}^* \dot{\boldsymbol{\eta}} + \mathbf{b} + \boldsymbol{\tau}^*) \quad (23)$$

$$= -\mathbf{s}^\top \mathbf{D}^* \mathbf{s} + \mathbf{s}^\top (-\mathbf{M}^* \ddot{\boldsymbol{\eta}}_r - \mathbf{D}^* \dot{\boldsymbol{\eta}}_r + \mathbf{b} + \boldsymbol{\tau}^*). \quad (24)$$

Now simplifying this expression by transforming the virtual reference velocity  $\boldsymbol{\nu}_r$  and acceleration  $\dot{\boldsymbol{\nu}}_r$  from the NED to BODY frame:

$$\boldsymbol{\nu}_r = \mathbf{R}^\top(\psi)\dot{\boldsymbol{\eta}}_r \quad (25)$$

$$\dot{\boldsymbol{\nu}}_r = \mathbf{R}^\top(\psi)(\ddot{\boldsymbol{\eta}}_r - \dot{\mathbf{R}}(\psi)\boldsymbol{\nu}_r). \quad (26)$$

For small motions,  $\dot{\mathbf{R}}(\psi) \approx \mathbf{0}$  and (24) can be written as:

$$\dot{V} = -\mathbf{s}^\top \mathbf{D}^* \mathbf{s} + \mathbf{s}^\top \mathbf{R}(\psi)(-\mathbf{M}\dot{\boldsymbol{\nu}}_r - \mathbf{D}\boldsymbol{\nu}_r + \mathbf{R}^\top(\psi)\mathbf{b} + \boldsymbol{\tau}_{SMC}). \quad (27)$$

In the implementation, the integral part of the sliding surface  $\mathbf{\Lambda}^\top \mathbf{\Lambda} \int_0^t \tilde{\boldsymbol{\eta}}(\tau) d\tau$  from (14) is multiplied with the gain matrix  $\mathbf{K}_d$  and added separately to the sum of control inputs. With this in mind, the control input is written as:

$$\begin{aligned} \boldsymbol{\tau}_{SMC} = & \underbrace{\hat{\mathbf{M}}\dot{\boldsymbol{\nu}}_r + \hat{\mathbf{D}}\boldsymbol{\nu}_r}_{\text{Feedforward term}} - \underbrace{\mathbf{R}^\top(\psi)\mathbf{K}_d\mathbf{s}}_{\text{PD-controller term}} \\ & - \underbrace{\mathbf{K}_s \cdot \times \tanh(\Phi^{-1}\mathbf{R}^\top(\psi)\mathbf{s})}_{\text{Robustifying term}}, \end{aligned} \quad (28)$$

where  $\hat{\mathbf{M}}$  is a chosen estimate of the system's inertia matrix and  $\hat{\mathbf{D}}$  is an estimate of the system's damping matrix. The gain matrix  $\mathbf{K}_d \in \mathbb{R}^{3 \times 3}$  with  $\mathbf{K}_d > 0$  is meant for tuning and is comparable with the derivative gain matrix used in PD control. The tuning matrix  $\mathbf{K}_s \in \mathbb{R}^{3 \times 3}$  with  $\mathbf{K}_s > 0$  is chosen as shown in (31) with  $\cdot \times$  as element-wise multiplication. Chattering is known to occur when using the  $\text{sgn}(\mathbf{R}^\top(\psi)\mathbf{s})$  function, causing oscillations around zero. The solution for solving this is to use a hyperbolic tangent function  $\tanh(\Phi^{-1}\mathbf{R}^\top(\psi)\mathbf{s})$  in order to reduce wear and tear of the vessel actuators. This function has the advantage of producing a smooth control input. The boundary layer matrix  $\Phi \in \mathbb{R}^{3 \times 3}$  with  $\Phi > 0$  is tunable and describes the boundary layer thickness for every DOF.

For simplicity, the integral action shown in (14) is assumed to still be a part of the sliding surface  $\mathbf{s}$ . With this in mind and by including  $\boldsymbol{\tau}$  from (28), the following is derived:

$$\begin{aligned} \dot{\mathbf{V}} = & -\mathbf{s}^\top(\mathbf{D}^* + \mathbf{K}_d)\mathbf{s} + \mathbf{s}^\top \mathbf{R}(\psi)(\mathbf{R}^\top(\psi)\mathbf{b} + \tilde{\mathbf{M}}\dot{\boldsymbol{\nu}}_r \\ & + \tilde{\mathbf{D}}\boldsymbol{\nu}_r - \mathbf{K}_s \cdot \times \tanh(\Phi^{-1}\mathbf{R}^\top(\psi)\mathbf{s})). \end{aligned} \quad (29)$$

Hence, we get:

$$\begin{aligned} \dot{\mathbf{V}} = & -\mathbf{s}^\top(\mathbf{D}^* + \mathbf{K}_d)\mathbf{s} + \mathbf{s}^\top \mathbf{R}(\psi)(\mathbf{R}^\top(\psi)\mathbf{b} + \tilde{\mathbf{M}}\dot{\boldsymbol{\nu}}_r \\ & + \tilde{\mathbf{D}}\boldsymbol{\nu}_r) - \underbrace{\mathbf{K}_s \cdot \times \mathbf{s}^\top \mathbf{R}(\psi) \|\tanh(\Phi^{-1}\mathbf{R}^\top(\psi)\mathbf{s})\|}_{\geq 0}, \end{aligned} \quad (30)$$

with  $\tilde{\mathbf{M}} = \hat{\mathbf{M}} - \mathbf{M}$  and  $\tilde{\mathbf{D}} = \hat{\mathbf{D}} - \mathbf{D}$ .

Choosing  $\mathbf{K}_s$  as:

$$\mathbf{K}_s \geq |\mathbf{R}^\top(\psi)\mathbf{b} + \tilde{\mathbf{M}}\dot{\boldsymbol{\nu}}_r + \tilde{\mathbf{D}}\boldsymbol{\nu}_r| + \delta, \quad \delta > 0 \quad (31)$$

where  $\mathbf{K}_s$  dominates the bias in addition to the error between estimated and actual inertia and damping uncertainties. The positive constant  $\delta$  ensures that  $\mathbf{K}_s > 0$ .

By applying (31), the time derivative of the Lyapunov function (30) becomes:

$$\begin{aligned} \dot{\mathbf{V}} \leq & -\mathbf{s}^\top(\mathbf{D}^* + \mathbf{K}_d)\mathbf{s} - \delta \|\mathbf{s}^\top \mathbf{R}(\psi)\| \|\tanh(\Phi^{-1}\mathbf{R}^\top(\psi)\mathbf{s})\| \\ & < 0, \quad \forall \mathbf{s} \neq \mathbf{0}. \end{aligned} \quad (32)$$

The Lyapunov function is negative definite when  $\mathbf{K}_s$  is chosen according to (31). Then the origin of the sliding surface  $\mathbf{s} = \mathbf{0}$  is exponentially stable. From (14) we know that  $\mathbf{s} = \mathbf{0}$  also means that the pose error  $\tilde{\boldsymbol{\eta}} = \mathbf{0}$  becomes exponentially stable.

#### 4. EXPERIMENTAL SETUP AND PERFORMANCE METRICS

This section describes the lab setup, test cases, controller tuning and performance metrics associated with model-scale tests on the Cybership 3 in the Marine Cybernetics

Laboratory (MCLab) at the Norwegian University of Science and Technology (NTNU).

##### 4.1 Marine Cybernetics Laboratory (MCLab) Setup

The MCLab is equipped with a water basin, DHI Wave Synthesizer wave generator, motion capture system including a motion camera PC and a vessel with a host PC as shown in Figure 1. The basin has the dimensions  $40 \times 6.5 \times 1.5 \text{ m}^3$ . Among different types of waves, the wave generator can generate irregular waves by pre-modeling and specifying wave parameters in the wave generator PC for the desired wave spectra. Wave parameters related to sea states generated in the MCLab are downscaled with Froude scaling (Steen, 2014) and the waves encounter the bow of the ship. Cybership 3 is a 1:30 scale model of a supply vessel and weighs 75 kg.

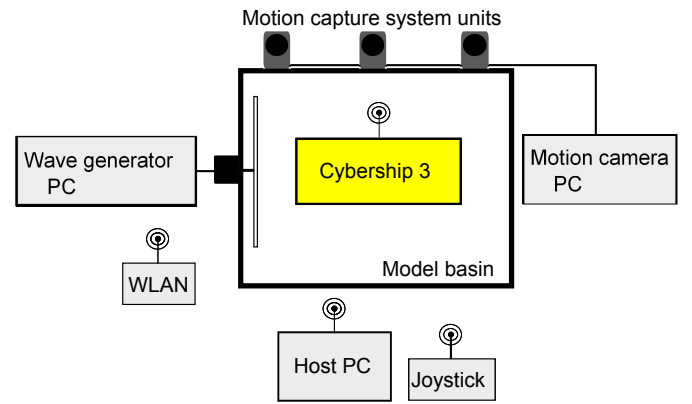


Fig. 1. Communication between all units in the MCLab.

A National Instruments CompactRio is mounted onboard Cybership 3 and communicates with the host PC, which has NI Veristand software through a WLAN connection. This computer is necessary for the operator to log and observe measurements, adjust controller settings and enable/disable the thrusters. Instrumentation onboard Cybership 3 provides acceleration measurements and are calibrated by lab staff. The measured acceleration used for the AFB-part of the PID-AFB controller is barely filtered by a low-pass filter due to very good measurements. The maximum measured variance of the acceleration was found to be  $\pm 0.0004 \text{ m/s}^2$ . The thrust allocation setup for Cybership 3 is shown in Figure 2. All azimuth thrusters were set in fixed positions and the third thruster was used to simulate a bow thruster as shown in the figure.

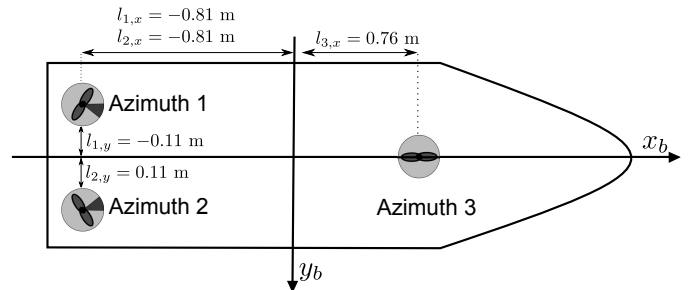


Fig. 2. Cybership 3 thrust allocation setup.

## 4.2 Test Cases

As mentioned in Section 3, the objective for Cybership 3 is to achieve  $\tilde{\boldsymbol{\eta}} \rightarrow \mathbf{0}$  when  $t \rightarrow \infty$ . This corresponds to station keeping at the center of the basin, 2 meters away from the wave flap. Test cases were performed in the MCLab with waves as the only environmental force, which were chosen to encounter the bow of the ship. For tuning purposes, the controllers were first tested in a calm sea state, providing a better basis for tuning prior to tests in extreme seas. First, the model-scaled sea state was calm with  $H_s = 0.03$  m and  $T_p = 0.8$  s, and afterwards the wave parameters were increased to  $H_s = 0.1$  m with  $T_p = 1.5$  s, which is referred to as rough (Price and Bishop, 1974). The latter is here referred to as extreme seas corresponding to  $H_s = 3.5$  m and  $T_p = 10$  s in full scale. The reason for not using larger wave heights and longer waves is due to limitations in the MCLab. The sea state still provides wave trains and couplings between the DOFs.

Tests related to the PID-AFB controller are found in Case 1, while Case 2 concerns tests with the SMC controller. Cases a-b in tables 2-3 were used for tuning in the calm sea state, while cases 1c-1f and 2c-2g were performed in extreme seas. The sea state parameters used in Case 1 and 2 are shown in Table 1.

Table 1: Sea state parameters.

Case	Significant wave height, $H_s$ [m]	Peak period of wave $T_p$ [s]	Description of sea
1a-1b, 2a-2b	0.03	0.8	Calm
1c-1f, 2c-2g	0.1	1.5	Extreme

## 4.3 Controller Tuning

The PID-AFB controller was tuned manually and the PID-part was tuned prior to the AFB-part. The tuning parameters are shown in Table 2 and they were also used to find tuning parameters for the SMC controller by comparing the PD-part of the PID-AFB control law (3) with the PD-controller term from (28) of the SMC control law. By choosing  $\mathbf{K}_{d,SMC}$  and  $\boldsymbol{\Lambda}$  of the SMC gain-matrices (34) with respect to the PD-part of the PID-AFB gain matrices (33) in the BODY frame, the controllers became more comparable in test cases:

$$\boldsymbol{\tau}_{PID} = -\mathbf{K}_p \tilde{\boldsymbol{\eta}} - \mathbf{K}_d \dot{\tilde{\boldsymbol{\eta}}} - \mathbf{K}_i \int_0^t \tilde{\boldsymbol{\eta}}(\tau) d\tau, \quad (33)$$

$$\begin{aligned} \mathbf{R}^\top(\psi) \boldsymbol{\tau}_{SMC,PD} &= -\mathbf{K}_d(\dot{\tilde{\boldsymbol{\eta}}} + 2\boldsymbol{\Lambda} \tilde{\boldsymbol{\eta}} \\ &+ \boldsymbol{\Lambda}^\top \boldsymbol{\Lambda} \int_0^t \tilde{\boldsymbol{\eta}}(\tau) d\tau), \end{aligned} \quad (34)$$

where

$$\mathbf{K}_{d,PID} = \mathbf{K}_{d,SMC}, \quad (35)$$

$$\mathbf{K}_{p,PID} = 2\mathbf{K}_{d,SMC} \boldsymbol{\Lambda}, \quad (36)$$

implying that

$$\boldsymbol{\Lambda} = (2\mathbf{K}_{d,SMC})^{-1} \mathbf{K}_{p,PID}. \quad (37)$$

By applying (35)-(37) with the gain matrices found in Table 2, the gain matrices  $\boldsymbol{\Lambda}$  and  $\mathbf{K}_d$  were found for the SMC. The gain matrix  $\mathbf{K}_s$  was found by satisfying (31) in combination with tuning. In addition, the boundary layer matrix  $\boldsymbol{\Phi}$  was found by tuning and is shown in Table 3 among the rest of the gain matrices.

The tuning parameter of interest for the PID-AFB controller is  $\Delta K$ , while overestimations of the inertia and damping matrices  $\mathbf{M}$  and  $\mathbf{D}$  are of interest for the SMC. Both controllers depend on more tunable parameters as shown in Table 2 and 3. In Table 2, the tuning parameter  $\Delta K$  provides an extra virtual inertia to the vessel that the control system uses during station keeping. This extra virtual inertia is tested with 0 kg, 10 kg, 30 kg and 50 kg. As shown in Table 3, estimations of the inertia and damping  $\hat{\mathbf{M}}$  and  $\hat{\mathbf{D}}$  are tested with 0%, +10%, +20%, +30%, +40%, +50%, because of increased model uncertainties, disturbances and added mass when Cybership 3 is exposed to extreme seas. By guessing such parameter uncertainties, the robustifying term (28) of the SMC control law has to dominate the errors induced by the feedforward terms in order to achieve the control objective. Considering that the PID-AFB strategy increases the virtual inertia of the system, it was reasonable to make the SMC inertia and damping matrix estimates larger than the real vessel parameters.

Table 2: Controller parameters for Case 1, PID-AFB.  $d\{\cdot \cdot \cdot\}$  denotes the diagonal matrix with values  $\cdot, \cdot, \cdot$  on the diagonal and zeros off the diagonal. Arrows indicate repetitive values.

Case	$\mathbf{K}_p$	$\mathbf{K}_d$	$\mathbf{K}_i$	Extra mass $\Delta K$ [kg]
1a	$d\{1.1 \ 1 \ 0.5\}$	$d\{5 \ 5 \ 5\}$	$d\{0.03 \ 0.06 \ 0.03\}$	0
1b	$d\{1.1 \ 1 \ 0.5\}$	$d\{5 \ 5 \ 5\}$	$d\{0.03 \ 0.06 \ 0.03\}$	30
1c	$d\{1.5 \ 1 \ 0.5\}$	$d\{8 \ 8 \ 8\}$	$d\{0.05 \ 0.1 \ 0.05\}$	0
1d				10
1e	↓	↓	↓	30
1f				50

Table 3: Controller parameters for Case 2, SMC.

Case	$\boldsymbol{\Lambda}$	$\mathbf{K}_d$	$\mathbf{K}_s$	$\boldsymbol{\Phi}$	Uncert. $\hat{\mathbf{M}}, \hat{\mathbf{D}}$ [%]
2a	$d\{0.03 \ 0.01 \ 0.2\}$	$d\{5 \ 5 \ 3\}$	$d\{1 \ 1 \ 1\}$	$d\{1 \ 1 \ 2\}$	0
2b	$d\{0.03 \ 0.01 \ 0.2\}$	$d\{5 \ 5 \ 3\}$	$d\{5 \ 1.3 \ 1.8\}$	$d\{1 \ 1 \ 2\}$	+30
2c	$d\{0.06 \ 0.03 \ 0.02\}$	$d\{13 \ 12 \ 5\}$	$d\{1 \ 1 \ 1\}$		0
2d			$d\{2 \ 1.5 \ 1.5\}$		+10
2e	↓	↓	$d\{5 \ 1.3 \ 1.8\}$	↓	+20
2f			$d\{6 \ 3 \ 2\}$		+40
2g			$d\{7 \ 4 \ 2.2\}$		+50

## 4.4 Performance metrics

In order to minimize error and improve PID-controller tuning, Murrill and Smith (1984) proposed three measures of performance, namely the integral of absolute value of error (IAE), integral of squared error (ISE) and integral of time multiplied by the absolute value of error (ITAE). But instead of using IAE, ISE and ITAE for tuning purposes, the cost functions are here used to quantify the performance of the PID-AFB and SMC controllers with respect to precision. Comparison of controllers with such performance metrics have been done in earlier work (Sørensen and Breivik, 2015). The IAE integrates the absolute error over time and does not add any weight to the errors:

$$IAE = \int_0^t |\epsilon| d\tau, \quad (38)$$

where  $\epsilon$  is the pose error. The ISE integrates the square of the error over time, meaning that large errors will be

penalized more than smaller ones:

$$ISE = \int_0^t \epsilon^2 d\tau. \quad (39)$$

The ITAE integrates the absolute error multiplied by time, such that errors which appear far into a time series will be penalized more than errors appearing early:

$$ITAE = \int_0^t \tau |\epsilon| d\tau. \quad (40)$$

In addition, a new cost function (42) is proposed, which is the product of one of the precision performance metrics (38)-(40) multiplied by the energy consumption of the thrusters for every time step during the test cases. This provides a combined measure of how precise the controller is with the energy consumption. A DP operation is green when the thrusters have low energy consumption and safe when the controller provides precise pose control. With this cost function, the measure of performance determines if the control strategy is smart by achieving the best possible combination of both a green and a safe operation. By logging the power consumption from each of the three thrusters on Cybership 3, the energy is found by:

$$E = \int_0^t P d\tau \quad (41)$$

The power was found by deriving relations between measured propeller rpm together with the motor constants for the thrusters. Defining  $\mathbf{E}_{tot} := \mathbf{E}_{thruster1} + \mathbf{E}_{thruster2} + \mathbf{E}_{thruster3}$  and  $\Upsilon$  as the measure of performance (38)-(40) with respect to  $\tilde{\boldsymbol{\eta}}$ , the new cost function becomes:

$$J_{\Upsilon} = \sum_{i=1}^n \mathbf{E}_{tot,i} \Upsilon_i \quad (42)$$

with  $n$  as the number of measurements for chosen simulation time and  $\Upsilon = \{ISE, IAE, ITAE\}$ .

## 5. EXPERIMENTAL RESULTS

Results from cases 1a-1f and 2a-2g have been evaluated by the new performance metric (42) and are shown in Table 4. As mentioned, cases 1a-1b and 2a-2b were meant for tuning purposes. When evaluating performance of 1a and 1b with  $J_{ISE}$ , the total cost from each case is compared and the best result is shown in Table 4. Case 1b provided

lower total cost than Case 1a, so Case 1b is shown in the table. Next, Case 2a and 2b has to be compared the same way. The tuning strategies providing best performance for PID-AFB and SMC in different sea states are compared. Lower total cost indicates better performance.

An increase of the inertia for the PID-AFB improved the performance for the calm sea state. The SMC provided best performance with no overestimations of the inertia and damping, acting as a pure PID controller.

However, when exposing the vessel to extreme seas, the control strategies for PID-AFB and SMC had to be changed. As shown in Table 4, increasing the inertia and uncertainties with the PID-AFB and SMC controllers provided better performance.

Table 4: The best performance out of all test cases for PID-AFB and SMC. Tests performed in the calm sea state are shown above the mid line while tests performed in extreme seas are shown below. The gray/white marked rows are test cases evaluated by the same performance metric.

Cost Type	Sea State	Controller Type	Extra Mass/Uncertainty [kg] / [%]	Case	Total Cost $J_{\Upsilon}$
$J_{ISE}$		PID-AFB	30	1b	0.04
$J_{ISE}$		SMC	0	2b	0.02
$J_{IAE}$	$H_s = 0.03$ m	PID-AFB	30	1b	2.18
$J_{IAE}$	$T_p = 0.8$ s	SMC	0	2a	1.55
$J_{ITAE}$		PID-AFB	30	1b	356
$J_{ITAE}$		SMC	0	2a	268
$J_{ISE}$		PID-AFB	30	1e	0.29
$J_{ISE}$		SMC	40	2f	0.15
$J_{IAE}$	$H_s = 0.1$ m	PID-AFB	30	1e	7.01
$J_{IAE}$	$T_p = 1.5$ s	SMC	40	2f	5.16
$J_{ITAE}$		PID-AFB	30	1e	1267
$J_{ITAE}$		SMC	40	2f	960

By examining Table 4, the SMC is seen to provide the best performance overall compared with PID-AFB control. In particular, Case 2f gave the best set of tuning parameters and an excerpt from the pose time series is shown in Figure 3 where the SMC was tuned with +40% uncertainty of the inertia and damping matrices. The controller is able to maintain a stable oscillation around the desired pose (red line). The heading shows that the vessel experiences wave

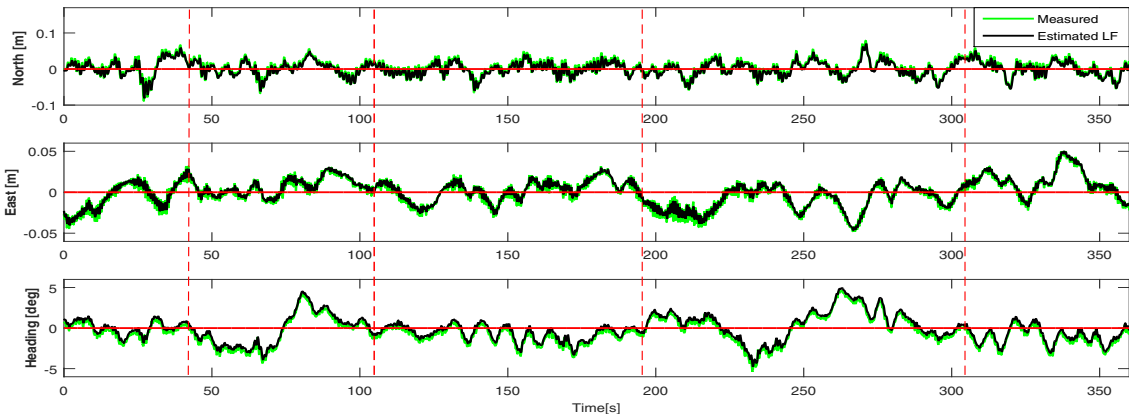


Fig. 3. Pose from Case 2f, SMC with +40% uncertainty of  $\mathbf{M}$  and  $\mathbf{D}$ . Significant wave height  $H_s = 0.1$  m and peak period of wave  $T_p = 1.5$  s. Marked intervals shows oscillations as a result of wave trains.

trains that may be observed by the oscillations during the periods 42-105 s and 195-305 s.

## 6. CONCLUSION

PID with acceleration feedback and sliding mode control were designed and implemented on the model-scale ship Cybership 3 in the Marine Cybernetics Laboratory at the Norwegian University of Science and Technology. The performance of the controllers were compared when operating with ship station keeping in extreme seas using new performance metrics combining pose accuracy with energy consumption. Sliding mode control provided the best performance when overestimating the inertia and damping matrices by +40%. For future work, the test cases may be extended by exposing Cybership 3 to waves encountering the vessel in more challenging angles than directly towards the bow. For example, waves may encounter the vessel at 30 degrees off the bow from either side. In addition, more uncertainties and estimations of the inertia and damping matrices may be tested.

## 7. ACKNOWLEDGMENTS

This work was supported by the Research Council of Norway through the Centres of Excellence funding scheme, project number 223254.

## REFERENCES

- Arimoto, S. and Miyazaki, F. (1984). Stability and Robustness of PID Feedback Control of Robot Manipulators of Sensory Capability. In M. Brady and R. Paul (eds.), *The 1st International Symposium on Robotics Research*, 783–799. MIT Press, Cambridge, MA, USA.
- Brodtkorb, A.H., Sørensen, A.J., and Teel, A.R. (2014). Increasing the operation window for dynamic positioned vessels using the concept of hybrid control. In *Proceedings of the International Conference on Ocean, Offshore and Arctic Engineering*. San Francisco, California, USA.
- Fossen, T.I. and Foss, B.A. (1991). Sliding control of MIMO nonlinear systems. *Modeling, Identification and Control*, 12(3), 129–138.
- Fossen, T.I. (2011). *Handbook of Marine Craft Hydrodynamics and Motion Control*. Wiley.
- Fossen, T.I., Skjetne, R., and Lindegaard, K.P.W. (2002). Inertia shaping techniques for marine vessels using acceleration feedback. In *Proceedings of the 15th IFAC World Congress*. Barcelona, Spain.
- Khalil, H.K. (2002). *Nonlinear Systems*. Prentice Hall.
- Lindegaard, K.P.W. (2003). *Acceleration Feedback in Dynamic Positioning*. Ph.D. thesis, Norwegian University of Science and Technology, Trondheim, Norway.
- Murrill, P. and Smith, C. (1984). *Automatic Control of Processes*. American Institute of Chemical Engineers.
- Nguyen, T.D., Sørensen, A.J., and Quek, S.T. (2007). Design of hybrid controller for dynamic positioning from calm to extreme sea conditions. *Automatica*, 43(5), 768–785.
- Price, W.G. and Bishop, R.E.D. (1974). *Probabilistic Theory of Ship Dynamics*. Chapman and Hall.
- Rabanal, O.M.R. (2015). *Comparing Controllers for Dynamic Positioning of Ships in Extreme Seas*. Master's thesis, Norwegian University of Science and Technology, Trondheim, Norway.
- Slotine, J. and Li, W. (1991). *Applied Nonlinear Control*. Prentice Hall.
- Sørensen, A.J. (2013). *Marine Control Systems: Propulsion and Motion Control of Ships and Ocean Structures, Lecture Notes*. Department of Marine Technology, Norwegian University of Science and Technology, Trondheim, Norway.
- Sørensen, A.J., Strand, J.P., and Nyberg, H. (2002). Dynamic positioning of ships and floaters in extreme seas. In *Proceedings of MTS/IEEE OCEANS'02*. Biloxi, Mississippi, USA.
- Sørensen, M.E.N. and Breivik, M. (2015). Comparing nonlinear adaptive motion controllers for marine surface vessels. In *Proceedings of the 10th IFAC Conference on Manoeuvring and Control of Marine Craft*. Copenhagen, Denmark.
- Steen, S. (2014). *Experimental Methods in Marine Hydrodynamics, Lecture Notes*. Department of Marine Technology, Norwegian University of Science and Technology, Trondheim, Norway.